Published in final edited form as:
Calcif Tissue Int. 2011 April ; 88(4): 325–335. doi:10.1007/s00223-010-9457-x.

Osteoblast Response to Ovariectomy Is Enhanced in Intrinsically High Aerobic-Capacity Rats

G. C. Goulet,
Department of Orthopaedic Surgery, University of Michigan, 2015 Biomedical Science Research Building, 109 Zina Pitcher Place, Ann Arbor, MI 48109-2200, USA

N. R. Halonen,
Department of Orthopaedic Surgery, University of Michigan, 2015 Biomedical Science Research Building, 109 Zina Pitcher Place, Ann Arbor, MI 48109-2200, USA

L. G. Koch,
Department of Anesthesiology, University of Michigan, Ann Arbor, MI 48109-2200, USA

S. L. Britton,
Department of Anesthesiology, University of Michigan, Ann Arbor, MI 48109-2200, USA

R. F. Zernicke, and
Department of Orthopaedic Surgery, School of Kinesiology, University of Michigan, Ann Arbor, MI 48109-2200, USA

K. M. Kozloff
Department of Orthopaedic Surgery, University of Michigan, 2015 Biomedical Science Research Building, 109 Zina Pitcher Place, Ann Arbor, MI 48109-2200, USA

K. M. Kozloff: kenkoz@umich.edu

Abstract

The role of exercise in promoting bone health is typically attributed to increased mechanical loading, which induces functional adaptation. Recent evidence suggests that habitual aerobic exercise has influence at the cellular level as well. The effect of aerobic capacity on osteoblast-lineage cell differentiation and function as well as skeletal phenotype is unknown. Using a rat model of high-capacity and low-capacity runners (HCRs and LCRs, respectively), in which an intrinsic functional genomic difference in aerobic capacity exists between nontrained animals, this study evaluated the effects of aerobic capacity on measures of bone mass and strength as well as osteoblast activity following ovariectomy. The ovariectomized rat emulates the clinical features of the estrogen-depleted human skeleton and represents a valuable model for studying short-term upregulation of osteoblast activity. We hypothesized that intrinsically high aerobic capacity would augment osteoblast response, which would mitigate the deleterious effects of hormone withdrawal. Femora and tibiae were assessed by micro-computed tomography, mechanical testing, and dynamic histomorphometry. HCRs had enhanced femoral tissue mineral density and estimated elastic modulus relative to LCRs. At 4 weeks postovariectomy, HCRs demonstrated a more robust osteoblast response. Markers of bone formation were upregulated to a greater extent in HCRs than LCRs, suggesting a role for aerobic capacity in governing osteoblast activity. Results from this and future studies will help to identify the influence of cellular aerobic metabolism on bone health, which may lead to new strategies for targeting diseases of the skeleton.

Correspondence to: K. M. Kozloff, kenkoz@umich.edu.

The authors have stated that they have no conflict of interest.

Keywords

Osteoporosis; Aerobic capacity; Bone metabolism; Ovariectomy; Osteoblast

Exercise plays an important role in regulating bone health, but the underlying mechanisms are still being described. The role of exercise in promoting bone health is typically attributed to increased mechanical loading, which induces functional adaptation. However, chronic aerobic exercise in particular can influence aerobic capacity at the cellular level. Skeletal muscle adapts to exercise through a regulated process that involves mitochondrial biogenesis in response to increased energy demands [1]. Additional mitochondria and enhanced oxidative enzyme activity provide the cellular basis for enhanced aerobic capacity. Recent evidence suggests that these intracellular exercise-induced adaptations in mitochondria are not limited to skeletal muscle. In rodent models, chronic endurance exercise induced mitochondrial biogenesis in multiple distant organs, including the brain, liver, heart, and kidney [2]. In aging mice, exercise prevents age-related decrements in the mitochondrial components of the liver and brain [2]. A full exploration of aerobic capacity effects on mitochondrial mass and function in tissues other than muscle has yet to be described [3]. Specifically, the effect of aerobic capacity on osteoblast-lineage cells is unknown, and it is unclear if differences in aerobic capacity of the osteoblast will affect cell differentiation and function as well as skeletal phenotype. Distinguishing skeletal effects due to cellular aerobic capacity from effects due to mechanical loading is challenging as during exercise the two occur concomitantly. Development of an animal model in which there are intrinsic, untrained differences in aerobic capacity would allow aerobic capacity differences to be investigated independently of an exogenous mechanical stimulus.

The Koch-Britton rat model of high-capacity and low-capacity runners (HCRs and LCRs, respectively) [4] has been used to test the global hypothesis that impaired oxygen metabolism is a common feature that mechanistically underlies multiple disease risks. Untrained rats were selectively bred over several generations for intrinsically high or low endurance running capacity, thereby providing a unique method for examining the phenotypic effects of altered aerobic metabolism. Rats phenotyped at generations 15–20 demonstrated that low aerobic capacity is associated with a greater risk for cardiovascular disease, anxiety, depression, and features of metabolic syndrome [5–7]. Therefore, the ability of cells to sense, utilize, and optimize oxygen through an aerobic pathway may represent a dominant factor in overall resistance to disease. Since cells of the osteoblast lineage are particularly responsive and sensitive to their local oxygen environment [8, 9], inherent intracellular aerobic capacity may induce downstream effects on bone cell function and skeletal phenotype.

Our preliminary studies on the role of aerobic metabolism on bone cell activity and function in vivo demonstrated that femoral tissue mineral density and estimated elastic modulus were significantly greater in HCRs relative to LCRs [10]. To eliminate potential effects on cells from confounding factors inherent to HCRs and LCRs, osteoblast progenitor cells were harvested from HCR and LCR rats and cultured in vitro. Osteoblast-lineage cells from HCR rats showed clear differences compared to LCRs, with greater cell numbers and increased mineralization and nodule size [11].

To further elucidate the role of inherent organism aerobic capacity in bone health, the current study examined the differential response of mature HCR and LCR rats to hormone withdrawal following ovariectomy (OVX). The OVX rat is a valuable preclinical model that emulates the features of the estrogen-depleted human skeleton. The site-specific development of cancellous osteopenia following OVX is one of the best-characterized

responses in skeletal research [12]. Importantly, because of the highly coupled activity of osteoclasts and osteoblasts, OVX also induces a significant and rapid increase in bone formation [e.g., 13, 14]. Consequently, the OVX rat represents a useful model for studying the short-term upregulation of osteoblast activity of HCR and LCR animals in response to duress (i.e., hormone withdrawal). We hypothesized that intrinsically high aerobic capacity would enhance osteoblast activity and mitigate the deleterious effects of hormone withdrawal following OVX. These results would lend further support to the global premise that inherent aerobic capacity of osteoblast-lineage cells is a significant factor in osteoblast differentiation and function as well as skeletal phenotype. These findings may suggest an alternate pathway responsible for the mediation of bone metabolism that normally accompanies aerobic exercise.

Methods

Animals

Twenty-four (12 HCRs, 12 LCRs) 30-week-old female rats from generation 24 of the Koch-Britton rat colony were randomly divided into two groups: bilaterally ovariectomized (OVX, $n = 6$ for HCRs and LCRs) and sham-operated (sham, $n = 6$ for HCRs and LCRs). Animals were given ad libitum access to food and de-ionized water at all times. Rats were pair-housed with animals from the same surgery group and monitored regularly for general health and adverse side effects resulting from surgery. Rats in all groups were administered 1% solutions of calcein (30 mg/kg, Sigma C0875; Sigma-Aldrich, St. Louis, MO) and alizarin (30 mg/kg, Sigma A3882; Sigma-Aldrich) 9 and 2 days prior to death, respectively. Four weeks after surgery, rats were killed with an overdose of pentobarbital. All procedures used in this study were approved by the University Committee on Use and Care of Animals at the University of Michigan.

Bilateral Ovariectomy

Rats were anesthetized with isofluorane and placed on a heating pad to maintain body temperature. The back of the anesthetized rat was shaved and aseptically prepared. A dorsal lateral incision was made, the right ovary located, and a suture placed around the ovarian artery and vein. The right ovary was removed distal to the suture, and the incision was glued and stapled closed. The same procedure was repeated to remove the left ovary and performed on the sham animals except that both ovaries were exteriorized and then replaced in the abdominal cavity.

Preparation of Bone Samples

Tibiae and femora were excised and cleaned of soft tissue. The right tibiae and femora were fixed in 10% neutral buffered formalin for 48 h and then transferred to 70% ethanol. These bones were dehydrated in a series of ethanol (70–100%) and embedded undecalcified in polymethyl-methacrylate (PMMA; Scientific Polymer Products, Ontario, NY). Thick sections (~ 400 μm) of the proximal tibial metaphysis (PTM) and femoral diaphysis were cut in the coronal and transverse planes, respectively, with a 100-μm diamond band saw (Exakt Technologies, Oklahoma City, OK), ground to a thickness of ~50 μm, and mounted on slides.

The left tibiae and femora were wrapped in saline-soaked gauze and stored at −20°C until analysis.

Dynamic Histomorphometry

Images were taken of the femoral diaphyseal and proximal tibial metaphyseal slides (described above) using a Zeiss Axiovert 200 M microscope (Carl Zeiss MicroImaging,

Thornwood, NY) with a Zeiss ApoTome (produces deblurred optical sections in thicker samples) and an X-Cite 120 fluorescent illumination system (Exfo Life Sciences Division, Missassauga, Canada). For trabecular measurements of the proximal tibial metaphysis, ~4 mm^2 of bone tissue was analyzed from one coronal section 1 mm distal from the proximal growth plate and 0.5 mm from the endocortical surface. Cortical measurements of the femoral diaphysis were taken from one transverse section located at the halfway point between the lesser trochanter and the distal growth plate. All images were acquired at 10× magnification and imported into Bioquant image analysis software (Bioquant Image Analysis, Nashville, TN). Histomorphometric measurements of trabecular and cortical bone included bone perimeter (B.Pm), single-label perimeter (sL.Pm), double-label perimeter (dL.Pm), and interlabel width (Ir.L.W). From these primary data, the following measurements were calculated for trabecular bone and the periosteal surface of cortical bone: mineralizing surface (MS/BS = [1/2sL.Pm + dL.Pm]/B.Pm; %), mineral apposition rate (MAR = Ir.L.W/7 days; μm day^{-1}), and bone formation rate (BFR/BS = MAR 9 MS/BS; $\mu m^3\ \mu m^{-2}\ day^{-1}$).

Quantitative Micro-Computed Tomography

Left tibiae and femora were scanned (Explore Locus SP; GE Healthcare, Waukesha, WI) and reconstructed at an isotropic voxel size of 30 μm. A calibration phantom was scanned before each session to provide quantitative data and account for day-to-day fluctuations in system parameters. Four regions of interest (ROI) were created: the tibial and femoral diaphyses, the proximal tibial metaphysis, and the femoral neck. The femoral diaphyseal ROI was 15% of the femoral length in height and centered at the halfway point between the lesser trochanter and the distal growth plate. The tibial diaphyseal ROI was 10% of the tibial length and positioned such that the distal boundary was 300 μm proximal to the tibia–fibula junction. The proximal tibial metaphysis was contoured manually to create an ROI consisting of trabecular bone 5% of the tibial length in height and positioned with its proximal boundary 1 mm distal to the proximal growth plate. The entire femoral neck was manually cropped and segmented into cortical and trabecular regions.

For analysis of each ROI, the following global thresholds were selected and used for all samples: 2,000 Houndsfield units (HU) for the tibial and femoral diaphyses; 1,200 HU for the proximal tibial metaphysis; and 2,300 and 1,500 for the trabecular and cortical regions of the femoral neck, respectively. Geometric measurements included cortical cross-sectional area (Ct.A), marrow area (Ct.MA), mean thickness (Ct.Th), and cross-sectional moment of inertia about the medial-lateral axis (I_{xx}) and trabecular bone volume fraction (BVF), spacing (Tb.Sp), and number (Tb.N). Trabecular and cortical tissue mineral density (Tb.TMD and Ct.TMD, respectively) were also evaluated.

Mechanical Testing

Biomechanical properties were assessed by three-point bending of the femur, torsion testing the tibia, and cantilever bending of the femoral neck. On the day of mechanical testing, bones were thawed to room temperature and kept wrapped in saline-soaked gauze until testing. For three-point bending, femora were placed on supports (1 mm radius at tip, 15 mm span) of a material testing machine (MTS Systems, Eden Prairie, MN) and stabilized using a static preload of 10 N before being loaded to failure with a crosshead (1 mm radius at tip) speed of 0.5 mm s^{-1}. Force and displacement data were collected at 200 Hz; and maximal load (N), stiffness (N mm^{-1}), and energy to failure (Nmm) were derived. An estimated elastic modulus (E_e) was calculated using

$$E_e = \frac{F}{d}\frac{L^3}{48 I_{xx}} \quad (1)$$

where F was the applied force, d the displacement of the crosshead, L the span of the supports, and I_{xx} the second moment of area with respect to the bending axis [15].

To perform the torsion test, the ends of the tibia were embedded in brass pots using a low-melting temperature Cerro alloy (McMaster-Carr, Chicago, IL) and mounted into a custom torsion-testing device, described previously [16]. The bones were tested in external rotation at a constant angular displacement of 0.5° s^{-1} until failure. Torque and displacement data were recorded at 1,000 Hz, and maximal torque (Nmm), stiffness (Nmm deg^{-1}), and energy to failure (Nmm deg) were derived.

Cantilever bending of the femoral neck followed methods detailed previously [17]. Briefly, the proximal portion of the fractured femur from three-point bending was embedded in a brass pot up to the level of the lesser trochanter using a Cerro alloy. A photograph (Panasonic G1; Panasonic, Secaucus, NJ) of each potted femur was taken for measurement of the cervical-diaphyseal angle, γ (i.e., angle between femoral neck and diaphyseal shaft). After photographing, the potted femur was secured in a custom base that allowed the femoral head to be positioned such that the femur was loaded in cantilever bending by a flat-surfaced probe (2.5 mm diameter) in a mechanical testing machine. A 2-N preload was applied, followed by testing with a constant crosshead speed of 0.5 mm s^{-1} until failure. Force and displacement data were collected at 1,000 Hz, and maximual load (N), stiffness (N mm^{-1}), and energy to failure (Nmm) were derived. Immediately after mechanical testing, the embedded portion of the fractured femora was photographed again to determine the moment arm of the bending force (r) and the fracture angle (α; i.e., angle between fracture surface and vertical). In addition, the fractured femoral heads were scanned using micro-computed tomography. Images of the fractured surfaces were acquired from the scans and imported into ImageJ 1.43r (National Institutes of Health, Bethesda, MD). Using a custom macro, fracture surface area (A), distance from the centroid to the superior surface (C), and second moment of area with respect to the bending axis (I) were calculated. With the combined morphological and mechanical data, maximal normal stress (σ_{max}) of the femoral neck was calculated using

$$\sigma_{max} = \frac{(F_{max} \sin \alpha)}{A} + \frac{[(F_{max} \cos \alpha) r] C}{I} \quad (2)$$

where F_{max} was the maximal applied force.

Statistical Analysis

Because animal body mass was a confounding factor [18], a two-factor general linear model with final body mass as a covariate was used to assess the significance of strain (HCR vs. LCR) and surgery (sham vs. OVX). Where body mass significantly predicted the dependent variable, body mass was evaluated in the model at a common value of 281.27 g. The interactive effects of strain and surgery were evaluated with a Bonferroni adjustment for multiple comparisons. These analyses were performed using IBM SPSS Statistics 18 (IBM, Chicago, IL). For dynamic histomorphometric measures, propagation of errors was used to calculate the mean and standard deviation for the difference between OVX and sham for HCRs and LCRs. Student's t-tests were used to compare HCRs and LCRs. For all tests, differences were considered significant at $P < 0.05$, and data were expressed as mean ± standard deviation. For all figures and tables, the following nomenclature was used to

identify significance: *significantly different between surgery and #significantly different between strain.

Results

Animal Characteristics

One animal was removed from the study (HCR OVX) due to the development of a large facial osteoma. At baseline, LCR animals were on average 30% heavier than HCRs ($P < 0.005$, Fig. 1). At the end of the study (4 weeks postsurgery), HCR OVX rats were 15.8% heavier than sham-treated rats ($P > 0.05$) and LCR OVX rats were 17.6% heavier than sham-treated rats ($P < 0.05$, Fig. 1). Final body mass of LCR animals was significantly greater than that of HCRs (sham +22.8%, $P < 0.05$; OVX +24.7%, $P > 0.01$).

Quantitative Micro-Computed Tomography

Femoral and tibial diaphyseal cortical morphology was significantly different between HCR and LCR animals (Table 1). Specifically, LCRs had significantly greater cortical area, marrow area, and second moment of area compared to HCRs. However, accounting for body mass as a covariate eliminated these differences (Table 1). After adjusting for body mass, the main effect of surgery was evident in the femoral diaphysis; cortical area was significantly greater in OVX animals ($P < 0.05$), and second moment of area was significantly reduced in HCR OVX ($P < 0.05$) relative to sham rats. Additionally, tibial diaphyseal cortical thickness was significantly greater in HCR animals ($P < 0.01$) compared to LCRs. However, conservative post hoc analysis did not reveal any significant interactive effects between strain and surgery for these measures.

Trabecular bone volume fraction in the proximal tibial metaphysis was significantly reduced in LCR OVX relative to sham rats (−32%, $P < 0.05$; Table 1; Fig. 2), whereas HCR animals appeared to be affected, although not significantly (−28%). Trabecular bone volume fraction in the femoral neck appeared to be greater in HCR OVX (+18%, $P > 0.05$) relative to sham animals, whereas BVF was lower in LCR OVX relative sham animals (−22%, $P > 0.05$).

Cortical and trabecular tissue mineral density were not different between sham and OVX animals (Table 1). By pooling HCR sham and OVX as well as LCR OVX and sham values, HCR demonstrated a 12% greater cortical tissue mineral density in the femoral diaphysis relative to LCRs (HCR 953.64 ± 139.48 mg cc^{-1}, LCR 850.65 ± 12.44 mg cc^{-1}; $P < 0.05$). In contrast, trabecular tissue mineral density of the proximal tibial metaphysis was significantly greater (5%) in LCR relative to HCR rats (HCR 449.71 ± 19.16 mg cc^{-1}, LCR 472.20 ± 20.06 mg cc^{-1}; $P < 0.05$).

Dynamic Histomorphometry

Dynamic histomorphometry results demonstrated the osteoblastic response to OVX in HCR and LCR rats. MS/BS and MAR in cortical bone of the femoral diaphysis and trabecular bone of the proximal tibial metaphysis were significantly greater in HCR and LCR OVX relative to sham animals (Table 2; Fig. 3). Consistently, BFR/BS was also significantly greater in HCR and LCR OVX rats relative to sham rats ($P < 0.001$; Table 2; Fig. 3). There were no significant differences in absolute levels between HCRs and LCRs for any of the dynamic histomorphometric measures. However, HCR OVX rats demonstrated a more robust upregulation of osteoblast activity compared to LCR OVX rats. The difference between OVX and sham femoral diaphyseal MS/BS, MAR, and BFR/BS was significantly greater in HCRs relative to LCRs (Table 2; Fig. 3). Proximal tibial metaphyseal MAR was also significantly upregulated to a greater extent in HCRs relative to LCRs.

Mechanical Testing

In general, LCR bone had greater mechanical properties than HCR (Fig. 4); the main effect of strain was significant for femoral diaphyseal maximal load ($P < 0.01$) and stiffness ($P = 0.001$), tibial diaphyseal maximal torque ($P < 0.01$) and energy to failure ($P < 0.01$), and femoral neck maximal load ($P < 0.001$). However, these structural-level differences were normalized with body mass as a covariate. After adjusting for LCRs' greater mass, femoral diaphyseal maximal load ($P < 0.028$) and femoral neck maximal load ($P < 0.039$) were significantly reduced in HCR and LCR OVX compared to sham animals.

At the material-level, estimated elastic modulus was not significantly different between sham and OVX animals (Fig. 4c). By pooling HCR sham and OVX as well as LCR OVX and sham values, HCRs had a 17% greater elastic modulus relative to LCRs (HCR 10.58 ± 1.53 GPa, LCR 9.04 ± 1.33 GPa; $P < 0.05$; Fig. 4c). Aside from the moment arm of bending, morphological properties of the femoral neck—used to calculate stress—were not significantly different between sham and OVX or HCR and LCR animals (Table 3). Maximal stress in the femoral neck was significantly greater in LCR sham relative to HCR sham rats ($P < 0.05$, Fig. 4i).

Discussion

This study examined for the first time the influence of intrinsically high aerobic capacity on bone mass and mechanical properties following OVX. Aerobic exercise capacity is a powerful predictor of mortality [19]. It was shown previously that rats with low aerobic capacity scored high on cardiovascular risk factors that constitute the metabolic syndrome [5]. Additionally, elevated oxidative capacity protected rats from high-fat diet-induced obesity and insulin resistance [6]. In general, high-aerobic capacity rats appear to be more resistant to disease and demonstrate decreased response to negative health environments. Previous studies suggest a more robust osteoblast phenotype in cells isolated from high-capacity animals [11]. We hypothesized that osteoblast activity would be enhanced in animals with intrinsically high aerobic capacity and that this would be protective against the deleterious effects of hormone withdrawal following OVX. Rats bred both for high- and low-endurance running capacity provided a genetic model with inherent differences in aerobic capacity that allowed for testing of this supposition without the confounding effects of a training stimulus. Additionally, the use of mature rats (7 months) ensured that OVX-induced effects (i.e., increased formation and loss of bone) could be separated from rapid growth in young animals (≤3 months) or age-related bone loss in old animals (≥9 months) [20].

The OVX rat is used widely as a model for the study of postmenopausal osteoporosis; the site-specific and time-dependent effects on the skeleton have been well-characterized [e.g., 21, 22]. Immediately following OVX, estrogen deficiency accelerates bone remodeling with a predominance of osteoclast activity over osteoblast activity, leading to the deterioration of bone mass and structure.

In the present study, at 4 weeks post-OVX, bone volume fraction at the proximal tibial metaphysis—the site of earliest statistically significant bone loss [12]—was 28% ($P > 0.05$) and 32% ($P < 0.05$) lower in HCR and LCR OVX animals, respectively, relative to sham (Table 1). This amount of bone loss in the proximal tibial metaphysis was consistent with previous studies [e.g., 21]. With respect to bone density, PTM tissue mineral density was reduced by 1.5 and 3.6% in HCR and LCR OVX animals, respectively, relative to sham, reflecting the increase in bone turnover levels and, thus, a greater percent of newer, less mineralized bone resulting from OVX.

The functional consequences of OVX were evaluated by biomechanical analyses of the femoral diaphysis and neck and the tibial diaphysis. After adjusting for body mass, femoral diaphyseal maximal load was significantly impacted by OVX ($P < 0.05$), although Bonferroni posttests did not reveal any significant interaction between strain and surgery. Tibial diaphyseal maximal torque was significantly reduced in LCR OVX animals ($P < 0.05$) relative to sham but not in HCRs. The lack of further loss in biomechanical competence was likely attributable to the slow loss of mechanistically important cortical bone following OVX [23]. In fact, some studies have reported an early transient increase in bone strength at 3 months post- OVX and no significantly adverse effect on strength in the femoral diaphysis until 9 months post-OVX [e.g., 24–26].

A clinically relevant site at which to assess strength is the femoral neck, which consists of a cortical shell and a trabecular core. The trabecular region has been shown to contribute approximately 25% to the strength of the neck [27]. Consequently, as bone loss proceeds at a greater rate in trabecular bone than cortical bone following OVX, the femoral neck represents a more sensitive site at which to evaluate biomechanical integrity. At 4 weeks post-OVX, OVX significantly affected maximal load (main effect $P < 0.05$) and tended to decrease stiffness and maximal stress in both HCR and LCR OVX animals relative to sham animals (Fig. 4g–i). At 12 weeks post-OVX, Nakamura et al. [28] reported a significantly lower maximal fracture load (−29.3%), relative to the sham-control group, which was likely related to a decrease in cortical width that is typically statistically significant by approximately 90 days post-OVX [12].

After 24 generations of selective breeding for high and low aerobic running capacity, there were several differences between 30-week-old female HCR and LCR sham-operated rats. Most significantly, low-capacity animals were heavier and skeletally larger than their high-capacity counterparts (Fig. 1). Consequently, LCR bones tended to have greater structural-level mechanical properties. However, consistent with a previous study of generation-18 female rats [18], these differences were attributed to scaling effects as significance was eliminated after accounting for body mass as a covariate.

At the material level, a previous study of generation-18 male rats demonstrated a significantly greater estimated elastic modulus from three-point bending of the femur and significantly greater cortical tissue mineral density, thereby suggesting an alteration in HCR bone tissue composition vs. LCRs [10]. Consistently, in the present study, estimated elastic modulus and cortical tissue mineral density were significantly greater in the femoral diaphysis of HCR relative to LCR animals. Furthermore, tissue mineral density of the tibial diaphysis and the femoral neck (cortical and trabecular) tended to be greater in HCR animals.

The resulting bone structural phenotype of high- and low-capacity animals in response to bilateral OVX at 4 weeks postsurgery was not markedly discrepant. LCR OVX animals did experience a significant loss of bone in the proximal tibial metaphysis, whereas HCR OVX animals maintained 4% more bone volume relative to the percent decrease in LCR OVX. However, in absolute terms, HCR OVX bone volume fraction was less than that of LCR OVX, and HCR trabecular architecture appeared to be more affected by OVX as demonstrated by a greater increase in trabecular spacing and a decrease in trabecular number. Manske and colleagues' reported a similar trend toward improved trabecular architecture in the proximal tibial metaphysis of healthy LCR vs. HCR rats [18, 29]. Increased tissue mineral density observed at this site in the present study further supported enhanced proximal tibial metaphyseal trabecular bone in LCRs.

Interestingly, the femoral neck of HCR rats did not appear to be affected by OVX at 4 weeks postsurgery and, in fact, demonstrated a relative improvement in cortical and trabecular measures. Although not significant, HCR OVX had 5.2% greater cortical tissue mineral density, 5.4% greater cortical thickness, 17% greater trabecular bone volume fraction, and 3.5% greater trabecular tissue mineral density relative to sham animals. Consistent with other sites analyzed, LCR OVX animals experienced reduced bone mass and architecture—most notably, a 24% decrease in trabecular bone volume fraction. However, the ability of HCR rats to maintain bone in the femoral neck was not reflected in the biomechanical data; maximal stress was impacted to the same extent in HCR and LCR animals (−29% in HCR and LCR OVX relative to sham).

Osteoblast activity is upregulated in the OVX rat [14, 30–32]. At 4 weeks post-OVX, all dynamic histomorphometric measures (i.e., MS/BS, MAR, and BFR/BS) were significantly increased on the periosteal surface of the femoral diaphysis and in the trabecular region of the proximal tibial metaphysis in HCR and LCR OVX relative to sham animals (Fig. 3). OVX stimulated periosteal bone growth in the femur, whereas the endosteum exhibited increased bone resorption leading to an enlargement of the medullary canal (Table 1). Consequently, measures of bone formation were not quantified for the endosteal surface. While structural parameters were similar between HCRs and LCRs, mechanistically, a marked difference between high- and low-aerobic capacity animals was the osteoblast response at 4 weeks post-OVX (Table 2; Fig. 3). In the femoral diaphysis, the upregulation (i.e., OVX–sham) of mineral apposition rate—a measure of osteoblast activity—was significantly greater in HCRs compared to LCRs. Similarly, the increase in mineralizing surface—a measure of the number of active osteoblasts—was significantly greater in HCRs compared to LCRs. In the proximal tibial metaphysis, mineral apposition rate was significantly upregulated to a greater extent in HCRs vs. LCRs.

This heightened osteoblast response in HCR animals when challenged was corroborated by a previous in vivo study in which a 1-mm section of cortical bone was removed from the femoral diaphysis and stabilized by an internal fixator [33]. High-capacity animals generated a more robust fracture-healing response as demonstrated by a significantly greater mineralized callus volume (when normalized to body mass). In a parallel in vitro study, intrinsically high organism aerobic capacity increased the ability of osteoprogenitor cells to proliferate, differentiate, and mineralize bone matrix [33]. Furthermore, preliminary studies of generation-25 rats suggested that HCR osteoblast-lineage cells were more efficient, required less oxygen during differentiation and formation of bone matrix, and regulated their ATP production differently from LCR animals (data not presented).

While no significant differences were observed in dynamic histomorphometric measures between HCRs and LCRs in either sham or OVX, the divergent response to OVX challenge suggests that aerobic-capacity effects may be most prominent in times of high metabolic demand, such as during fracture repair or after OVX.

A change in an unselected trait produced by selection for another trait is termed a “correlated response.” Artificial selection for endurance capacity produced differences in body mass as a correlated trait in both sexes. In general, the low-capacity line became increasingly heavier and the high-capacity line increasingly lighter at each generation. As bone mass and strength tend to increase with body mass [34], this correlated divergence between high- and low-capacity rats confounded morphological, densitometric, and biomechanical data. However, importantly, the percent upregulation in osteoblast activity between sham and OVX animals indirectly accounts for body mass differences in that bone-formation rate is normalized by total bone surface.

Additionally, high- and low-aerobic capacity rats differed with respect to their levels of cage activity. In a previous study, high-capacity rats were 25% more active (determined by beam-breaks/minute over 24 h) than low-capacity rats [35]. Discrepant activity levels may have introduced differences in exogenous mechanical loading to the HCR and LCR skeletons. Beneficially, the increased body mass of the low-capacity animals would serve to mitigate rather than exacerbate the differences in external stimuli between the HCR and LCR animals used in this study.

A further consideration is the lack of baseline (i.e., presurgery) controls. However, using skeletally mature rats (6 months), Tou et al. [36] found no differences in growth or bone loss in baseline controls compared to sham-operated animals at the end of a 4-week study. Consequently, it is likely that in the present study the sham-operated controls represented normal development and that the differences observed between OVX and sham animals were primarily the result of estrogen withdrawal due to OVX.

This study aimed to identify the influence of intrinsic aerobic capacity on the response of the skeleton when challenged by OVX. Results corroborated previous findings that high-capacity rats have greater cortical tissue mineral density and estimated elastic modulus compared to their low-capacity counterparts. Additionally, osteoblast activity in vivo was highlighted as a potential protective mechanism against OVX-induced bone loss. The augmented osteoblast response in high-capacity animals lends further support to our global hypothesis that beneficial effects of organism aerobic capacity are not limited to skeletal muscle tissue but may extend to bone tissue and cells of the osteoblast lineage. Future studies will continue to explore the correlation among heightened osteoblast function and organism aerobic capacity in vitro and in vivo.

Acknowledgments

We are grateful to K. Sweet, B. Nolan, C. Roehm, D. Kayner, and C. Clifford for their contributions to this work. We thank the National Institutes of Health (grant R24 RR17718 to S. L. B. and L. G. K.) for partial funding support.

References

1. Davies KJ, Packer L, Brooks GA. Biochemical adaptation of mitochondria, muscle, and whole-animal respiration to endurance training. Arch Biochem Biophys. 1981; 209:539–554. [PubMed: 7294809]
2. Navarro A, Gomez C, Lopez-Cepero JM, Boveris A. Beneficial effects of moderate exercise on mice aging: survival, behavior, oxidative stress, and mitochondrial electron transfer. Am J Physiol Regul Integr Comp Physiol. 2004; 286:R505–R511. [PubMed: 14615275]
3. Boveris A, Navarro A. Systemic and mitochondrial adaptive responses to moderate exercise in rodents. Free Radic Biol Med. 2008; 44:224–229. [PubMed: 18191758]
4. Koch LG, Britton SL. Artificial selection for intrinsic aerobic endurance running capacity in rats. Physiol Genomics. 2001; 5:45–52. [PubMed: 11161005]
5. Wisloff U, Najjar SM, Ellingsen O, Haram PM, Swoap S, Al-Share Q, Fernstrom M, Rezaei K, Lee SJ, Koch LG, Britton SL. Cardiovascular risk factors emerge after artificial selection for low aerobic capacity. Science. 2005; 307:418–420. [PubMed: 15662013]
6. Noland RC, Thyfault JP, Henes ST, Whitfield BR, Woodlief TL, Evans JR, Lust JA, Britton SL, Koch LG, Dudek RW, Dohm GL, Cortright RN, Lust RM. Artificial selection for high-capacity endurance running is protective against high-fat diet-induced insulin resistance. Am J Physiol Endocrinol Metab. 2007; 293:E31–E41. [PubMed: 17341547]
7. Morris EM, Whaley-Connell AT, Thyfault JP, Britton SL, Koch LG, Wei Y, Ibdah JA, Sowers JR. Low aerobic capacity and high-fat diet contribute to oxidative stress and IRS-1 degradation in the kidney. Am J Nephrol. 2009; 30:112–119. [PubMed: 19229113]

8. Hirao M, Hashimoto J, Yamasaki N, Ando W, Tsuboi H, Myoui A, Yoshikawa H. Oxygen tension is an important mediator of the transformation of osteoblasts to osteocytes. J Bone Miner Metab. 2007; 25:266–276. [PubMed: 17704991]
9. Zahm AM, Bucaro MA, Srinivas V, Shapiro IM, Adams CS. Oxygen tension regulates preosteocyte maturation and mineralization. Bone. 2008; 43:25–31. [PubMed: 18485858]
10. Halonen, NR.; Cole, JH.; Goulet, GC.; Sobel, A.; Koch, LG.; Britton, SL.; Morris, MD.; Zernicke, RF.; Kozloff, K. Influence of intrinsic and trained aerobic capacity on bone mineralization and material properties. Transactions of the 56th Annual Meeting of the Orthopaedic Research Society; New Orleans, LA. 2010. 0069
11. Halonen, NR.; Tayim, R.; Goulet, GC.; Cole, JH.; Clifford, C.; Goldstein, SA.; Koch, LG.; Britton, SL.; Zernicke, RF.; Alford, AI.; Kozloff, K. Intrinsic aerobic capacity influences MSC proliferation, mineralization, and fracture healing. Transactions of the 56th Annual Meeting of the Orthopaedic Research Society; New Orleans, LA. 2010. p. 1712
12. Jee WS, Yao W. Overview: animal models of osteopenia and osteoporosis. J Musculoskelet Neuronal Interact. 2001; 1:193–207. [PubMed: 15758493]
13. Bagi CM, DeLeon E, Ammann P, Rizzoli R, Miller SC. Histo-anatomy of the proximal femur in rats: impact of ovariectomy on bone mass, structure, and stiffness. Anat Rec. 1996; 245:633–644. [PubMed: 8837721]
14. Sato M, Zeng GQ, Turner CH. Biosynthetic human parathyroid hormone (1–34) effects on bone quality in aged ovariectomized rats. Endocrinology. 1997; 138:4330–4337. [PubMed: 9322947]
15. Turner CH, Burr DB. Basic biomechanical measurements of bone: a tutorial. Bone. 1993; 14:595–608. [PubMed: 8274302]
16. Taylor DK, Meganck JA, Terkhorn S, Rajani R, Naik A, O'Keefe RJ, Goldstein SA, Hankenson KD. Thrombospondin-2 influences the proportion of cartilage and bone during fracture healing. J Bone Miner Res. 2009; 24:1043–1054. [PubMed: 19123916]
17. Hou JC, Zernicke RF, Barnard RJ. High fat–sucrose diet effects on femoral neck geometry and biomechanics. Clin Biomech (Bristol, Avon). 1990; 5:162–168.
18. Manske, SL.; Steiner, D.; Kim, SH.; Boyd, SK.; Koch, LG.; Britton, SL.; Hepple, RT.; Zernicke, RF. Differences in bone morphology in older female rats selectively bred for high and low aerobic capacity. Transactions of the 54th Annual Meeting of the Orthopaedic Research Society; San Francisco, CA. 2008. 0910
19. Myers J, Prakash M, Froelicher V, Do D, Partington S, Atwood JE. Exercise capacity and mortality among men referred for exercise testing. N Engl J Med. 2002; 346:793–801. [PubMed: 11893790]
20. Kalu DN. The ovariectomized rat model of postmenopausal bone loss. Bone Miner. 1991; 15:175–191. [PubMed: 1773131]
21. Wronski TJ, Cintron M, Dann LM. Temporal relationship between bone loss and increased bone turnover in ovariectomized rats. Calcif Tissue Int. 1988; 43:179–183. [PubMed: 3141020]
22. Wronski TJ, Dann LM, Scott KS, Cintron M. Long-term effects of ovariectomy and aging on the rat skeleton. Calcif Tissue Int. 1989; 45:360–366. [PubMed: 2509027]
23. Lelovas PP, Xanthos TT, Thoma SE, Lyritis GP, Dontas IA. The laboratory rat as an animal model for osteoporosis research. Comp Med. 2008; 58:424–430. [PubMed: 19004367]
24. Danielsen CC, Mosekilde L, Svenstrup B. Cortical bone mass, composition, and mechanical properties in female rats in relation, to age, long-term ovariectomy, and estrogen substitution. Calcif Tissue Int. 1993; 52:26–33. [PubMed: 8453502]
25. Mosekilde L, Sogaard CH, Danielsen CC, Torring O. The anabolic effects of human parathyroid hormone (hPTH) on rat vertebral body mass are also reflected in the quality of bone, assessed by biomechanical testing: a comparison study between hPTH-(1–34) and hPTH-(1–84). Endocrinology. 1991; 129:421–428. [PubMed: 2055197]
26. Aerssens J, van Audekercke R, Talalaj M, Geusens P, Bramm E, Dequeker J. Effect of 1alpha-vitamin D_3 and estrogen therapy on cortical bone mechanical properties in the ovariectomized rat model. Endocrinology. 1996; 137:1358–1364. [PubMed: 8625911]

27. Hou JC, Zernicke RF, Barnard RJ. Experimental diabetes, insulin treatment, and femoral neck morphology and biomechanics in rats. Clin Orthop Relat Res. 1991; 264:278–285. [PubMed: 1997247]

28. Nakamura Y, Naito M, Hayashi K, Fotovati A, Abu-Ali S. Effect of combined treatment with alendronate and calcitriol on femoral neck strength in osteopenic rats. J Orthop Surg Res. 2008; 3:51. [PubMed: 19091077]

29. Sharkey, NA.; Lang, DH.; Okita, N.; Koch, LG.; Britton, SL. Differences in bone morphology in older female rats selectively bred for high and low aerobic capacity. Transactions of the 52nd Annual Meeting of the Orthopaedic Research Society; Chicago, IL. 2006. p. 348

30. Oxlund BS, Ortoft G, Andreassen TT, Oxlund H. Low-intensity, high-frequency vibration appears to prevent the decrease in strength of the femur and tibia associated with ovariectomy of adult rats. Bone. 2003; 32:69–77. [PubMed: 12584038]

31. Yao W, Hadi T, Jiang Y, Lotz J, Wronski TJ, Lane NE. Basic fibroblast growth factor improves trabecular bone connectivity and bone strength in the lumbar vertebral body of osteopenic rats. Osteoporos Int. 2005; 16:1939–1947. [PubMed: 16086094]

32. Andresen CJ, Moalli M, Turner CH, Berryman E, Pero R, Bagi CM. Bone parameters are improved with intermittent dosing of vitamin D_3 and calcitonin. Calcif Tissue Int. 2008; 83:393–403. [PubMed: 19018584]

33. Halonen, NR.; Tayim, R.; Goulet, GC.; Cole, JH.; Clifford, C.; Goldstein, SA.; Koch, LG.; Britton, SL.; Zernicke, RF.; Alford, AI.; Kozloff, K. Intrinsic aerobic capacity influences MSC proliferation, mineralization, and fracture healing. Transactions of the 56th Annual Meeting of the Orthopaedic Research Society; New Orleans, LA. 2010. p. 1712

34. Frost HM. Obesity, and bone strength and “mass”: a tutorial based on insights from a new paradigm. Bone. 1997; 21:211–214. [PubMed: 9276084]

35. Novak CM, Escande C, Gerber SM, Chini EN, Zhang M, Britton SL, Koch LG, Levine JA. Endurance capacity, not body size, determines physical activity levels: role of skeletal muscle PEPCK. PLoS One. 2009; 4:e5869. [PubMed: 19521512]

36. Tou JC, Foley A, Yuan YV, Arnaud S, Wade CE, Brown M. The effect of OVX combined with hindlimb unloading and reloading on the long bones of mature Sprague-Dawley rats. Menopause. 2008; 15:494–502. [PubMed: 18030174]

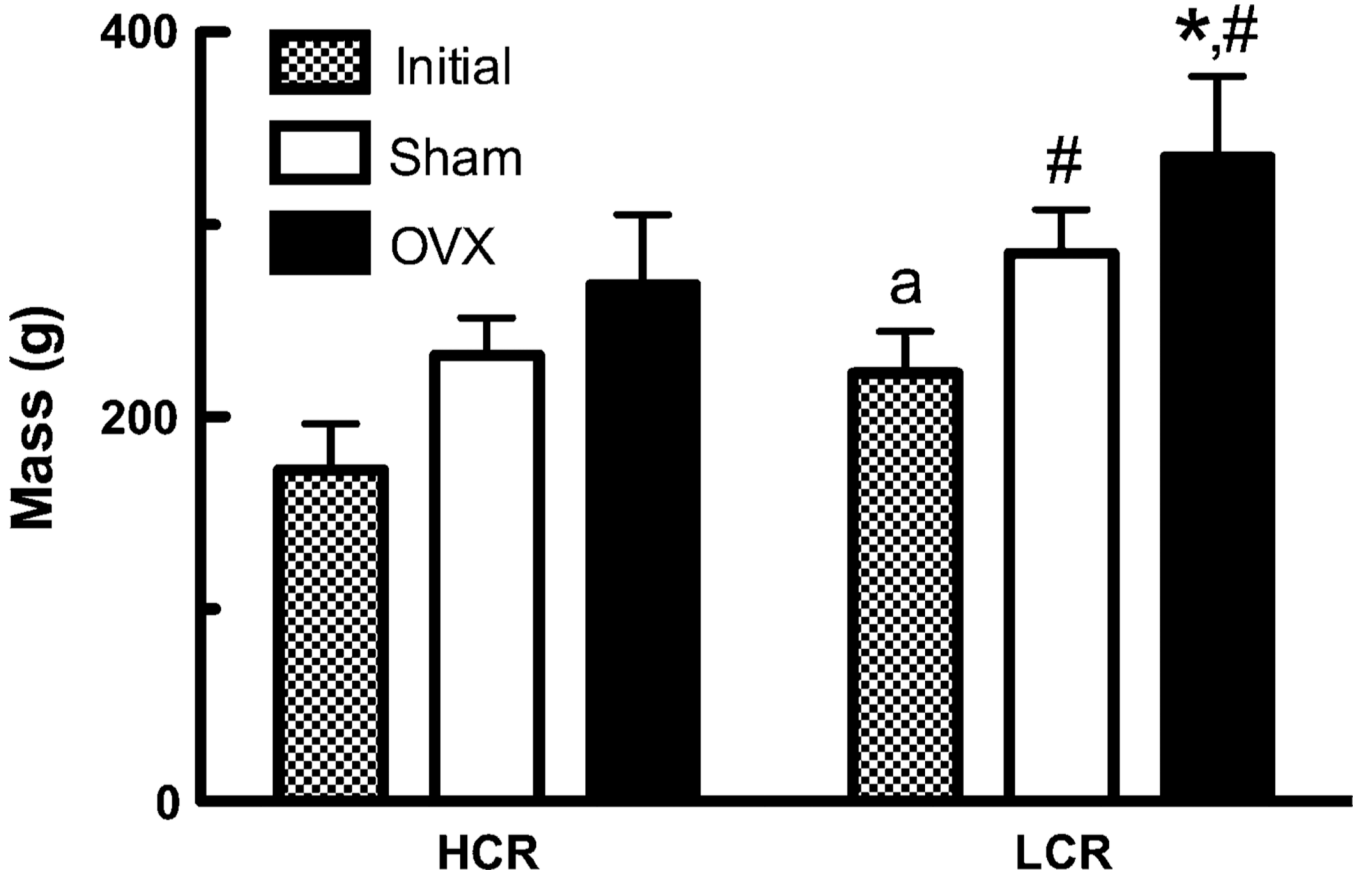

Fig. 1.

Animal body mass. Initial (HCR $n = 12$, LCR $n = 12$) and 4 weeks postsurgery (LCR sham and OVX $n = 6$, HCR sham $n = 6$, HCR OVX $n = 5$). [a] Significantly different between HCR and LCR initial body mass, * significantly different between surgery, [#] significantly different between strain

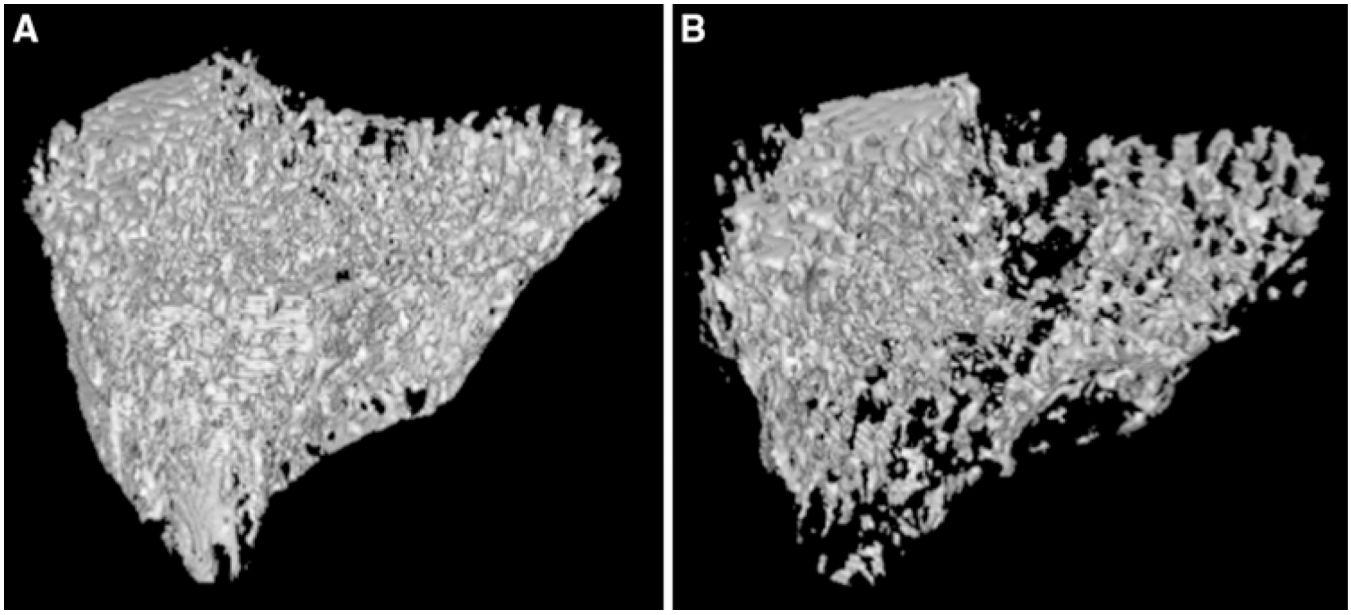

Fig. 2.
Three-dimensional renderings of trabecular bone from proximal tibia metaphysis from representative LCR a sham (BVF = 0.60) and b OVX (BVF = 0.41) rats

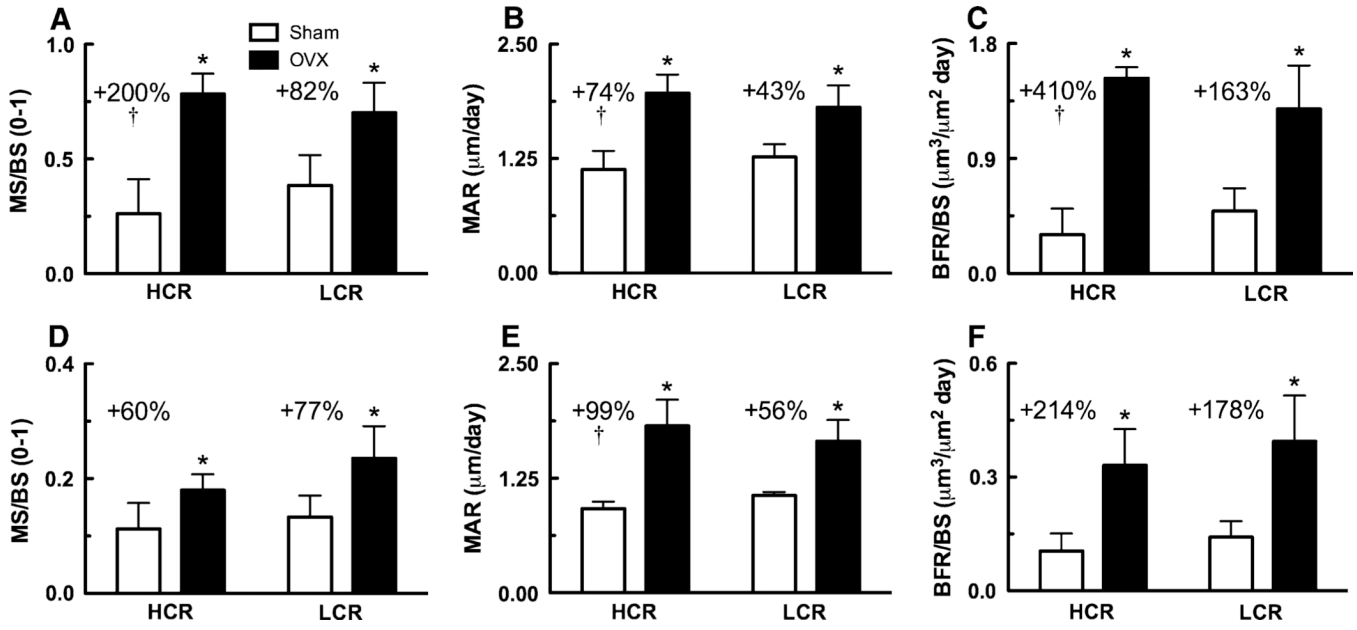

Fig. 3.

Dynamic histomorphometric measures from cortical bone of the femoral diaphysis and trabecular bone of the proximal tibial metaphysis. **a** Femoral diaphyseal periosteal (MS/BS), **b** mineral apposition rate (MAR), and **c** periosteal bone formation rate (BFR/BS). **d** Proximal tibial metaphyseal MS/BS, **e** MAR, and **f** BFR/BS. *Percentages* represent OVX levels relative to sham. † Upregulation of dynamic histomorphometric measure (i.e., OVX–sham) significantly greater in HCRs compared LCRs, * significantly different between surgery

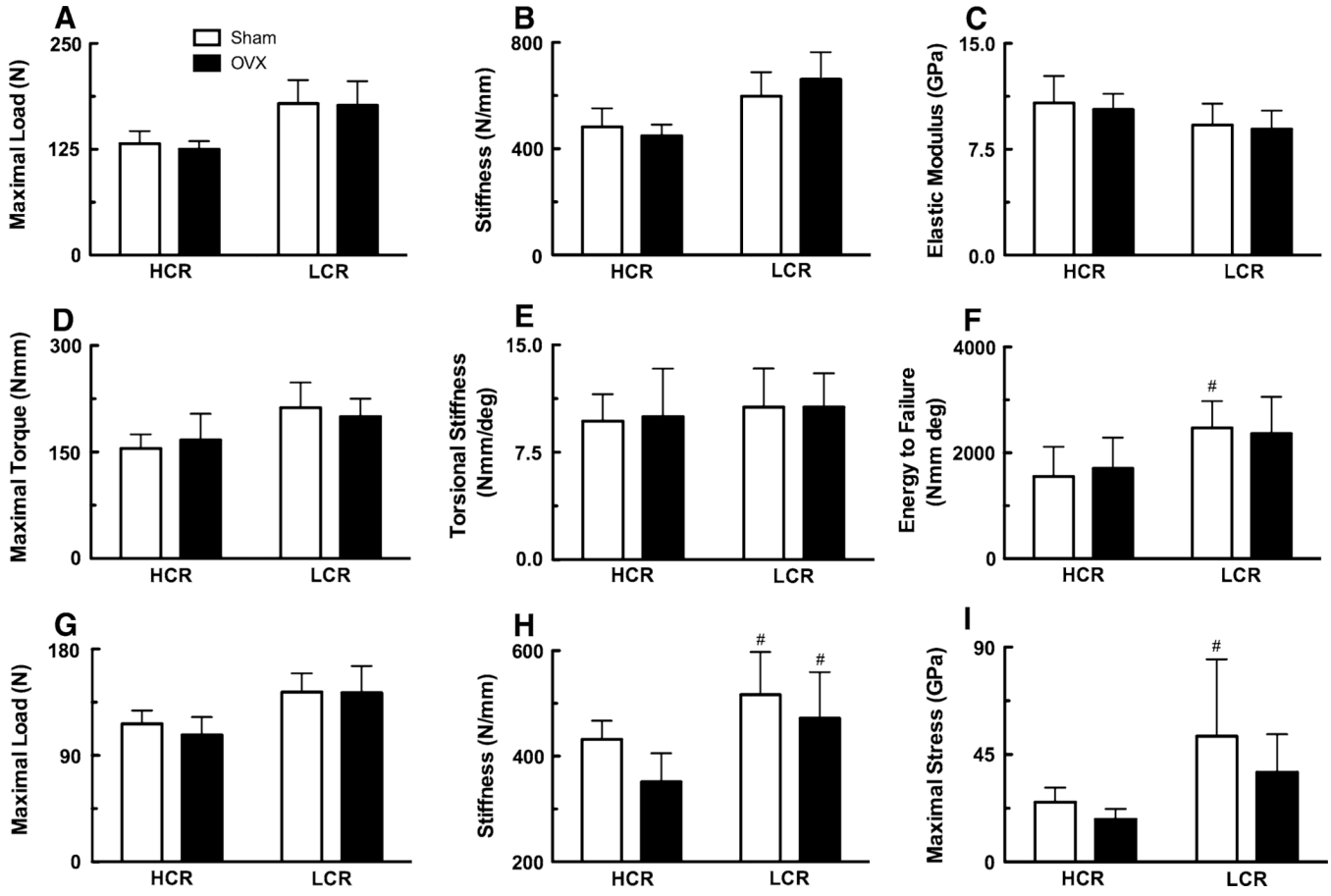

Fig. 4.

Mechanical properties of the femur and tibia. Femoral diaphyseal **a** maximum load, **b** stiffness, and **c** estimated elastic modulus. Tibial diaphyseal **d** maximum torque, **e** stiffness, and **f** energy to failure from torsion testing. Femoral neck **g** maximum load, **h** stiffness, and **i** maximum stress from cantilever bending. # Significantly different between strain

Table 1

Skeletal morphology and densitometry

Parameter	Body mass covariate	Main effect $P < 0.05$	Strain/surgery			
			HCR/sham ($n = 6$)	HCR/OVX ($n = 5$)	LCR/sham ($n = 6$)	LCR/OVX ($n = 6$)
Femoral diaphysis						
Ct.A (mm^2)	Sig.	Surgery	5.1 ± 0.47	5.16 ± 0.58	5.71 ± 0.56	5.92 ± 0.49
Ct.MA (mm^2)	Sig.	–	2.16 ± 0.55	2.30 ± 0.23	3.20 ± 0.29	3.33 ± 0.62
Ct.Th (mm)	Sig.	–	0.68 ± 0.04	0.69 ± 0.04	0.68 ± 0.05	0.69 ± 0.02
I_{xx} (mm^4)	Sig.	Surgery	3.19 ± 0.64	3.11 ± 0.59*	4.74 ± 0.76	5.33 ± 1.31
Ct.TMD (mg cc^{-1})	–	Strain	937 ± 142.7	979 ± 151.7	850.2 ± 12.6	851.1 ± 13.4
Tibial diaphysis						
Ct.A (mm^2)	Sig.	–	3.4 ± 0.26	3.58 ± 0.51	3.8 ± 0.34	4.05 ± 0.24
Ct.MA (mm^2)	Sig.	Strain	0.81 ± 0.14#	0.71 ± 0.12#	1.19 ± 0.07	1.15 ± 0.16
Ct.Th (mm)	Sig.	Strain	0.65 ± 0.04#	0.69 ± 0.07#	0.64 ± 0.04	0.68 ± 0.04
I_{xx} (mm^4)	Sig.	–	1.37 ± 0.16	1.45 ± 0.39	1.78 ± 0.30	2.04 ± 0.30
Ct.TMD (mg cc^{-1})	–	–	847.8 ± 13.7	863.4 ± 21.7	845.3 ± 6.9	849.5 ± 11.1
Proximal tibial metaphysis						
BVF	–	Surgery	0.54 ± 0.16	0.39 ± 0.15	0.61 ± 0.13	0.42 ± 0.06*
Tb.Sp (mm)	Sig.	Strain	0.09 ± 0.03#	0.18 ± 0.14#	0.08 ± 0.02	0.13 ± 0.02
Tb.N (N mm^{-1})	–	–	5.29 ± 0.81	4.53 ± 1.08	4.93 ± 0.53	4.59 ± 0.19
Tb.TMD (mg cc^{-1})	–	Strain	453 ± 20.6	445.9 ± 18.9	480.9 ± 25#	463.5 ± 16.2
Femoral neck						
Ct.A (mm^2)	–	–	2.2 ± 0.34	2.17 ± 0.07	2.37 ± 0.15	2.34 ± 0.19
Ct.Th (mm)	–	–	0.37 ± 0.07	0.39 ± 0.03	0.4 ± 0.035	0.38 ± 0.064
Ct.TMD (mg cc^{-1})	–	–	718.3 ± 90.7	755.8 ± 87.9	693.8 ± 13.2	689.8 ± 33.9
BVF	–	–	0.41 ± 0.19	0.48 ± 0.11	0.46 ± 0.13	0.35 ± 0.12
Tb.Sp (mm)	–	–	0.14 ± 0.046	0.14 ± 0.034	0.11 ± 0.021	0.15 ± 0.036
Tb.N (N mm^{-1})	–	–	5.35 ± 0.46	5.55 ± 0.42	6.08 ± 0.34	5.36 ± 1.13
Tb.TMD (mg cc^{-1})	–	–	740.5 ± 65.6	766.2 ± 67.7	720.7 ± 17.3	711.2 ± 22.8

Sig. represents significance ($P < 0.05$) of animal body mass as a covariate.

* Significantly different between surgery;

significantly different between strain

Table 2

Dynamic histomorphometry

Parameter	HCR			LCR		
	Sham (n = 6)	OVX (n = 5)	OVX–sham	Sham (n = 6)	OVX (n = 6)	OVX–sham
Femoral diaphysis						
Ps.MS/BS (%)	26.1 ± 15.1	78.4 ± 8.8*	0.52 ± 0.18†	38.5 ± 13.1	70.2 ± 13.0*	0.32 ± 0.18
Ps.MAR (μm day^{-1})	1.13 ± 0.20	1.97 ± 0.20*	0.83 ± 0.29†	1.27 ± 0.40	1.81 ± 0.24*	0.54 ± 0.28
Ps.BFR/BS (μm^3 μm^{-2} day^{-1})	0.30 ± 0.20	1.53 ± 0.09*	1.22 ± 0.22†	0.49 ± 0.18	1.29 ± 0.34*	0.80 ± 0.38
Proximal tibial metaphysis						
MS/BS (%)	11.2 ± 4.5	18.0 ± 2.8*	0.07 ± 0.05	13.3 ± 3.8	23.5 ± 5.6*	0.10 ± 0.07
MAR (μm day^{-1})	0.92 ± 0.08	1.82 ± 0.28*	0.91 ± 0.30†	1.06 ± 0.04	1.66 ± 0.23*	0.59 ± 0.23
BFR/BS (μm^3 μm^{-2} day^{-1})	0.10 ± 0.05	0.33 ± 0.10*	0.23 ± 0.11	0.14 ± 0.04	0.39 ± 0.12*	0.25 ± 0.13

†Upregulation of dynamic histomorphometric measure (i.e., OVX–sham) significantly greater (P < 0.05) in HCRs compared to LCRs.

*Significantly different between surgery

Calcif Tissue Int. Author manuscript; available in PMC 2012 March 8.

Table 3

Morphological properties of the femoral neck

Parameter	Strain/surgery			
	HCR/sham (*n* = 6)	HCR/OVX (*n* = 5)	LCR/sham (*n* = 6)	LCR/OVX (*n* = 6)
Cervical-diaphyseal angle	122.3 ± 1.3	121.9 ± 2.0	123.1 ± 1.9	124.4 ± 0.8
Fracture line-neck angle	18.7 ± 2.8	19.9 ± 1.4	18.3 ± 1.5	18.0 ± 3.1
Total bone cross-sectional fracture area (mm^2)	8.7 ± 0.7	9.5 ± 1.5	9.1 ± 2.2	9.7 ± 1.8
Moment arm of bending force (mm)	1.3 ± 0.2	1.1 ± 0.1	1.8 ± 0.2#	1.6 ± 0.3#
Second moment of bone area about bending axis (mm^4)	23.0 ± 6.4	26.5 ± 9.1	22.6 ± 14.5	28.3 ± 11.8

Significantly different between strain